

# Necking Mechanism and Its Elimination in Uniaxially Drawn Films of Poly(ethylene naphthalate) (PEN)/Polyetherimide (PEI) Blends

M. CAKMAK, J. C. KIM\*

Polymer Engineering Institute, University of Akron, Akron, Ohio 44325-0301

Received 6 August 1996; accepted 30 December 1996

**ABSTRACT:** The influence of blend composition on the deformation behavior of cast amorphous PEN/PEI blends were investigated above their respected glass transition temperatures. PEN inherently shows a sharp necking phenomenon when stretched at temperatures as high as 20°C above its glass transition temperature. This was attributed to highly localized rapid alignment of naphthalene planes parallel to the surface of the films. The addition of PEI was observed to reduce this necking behavior. The neck formation completely disappears when the PEI fraction exceeds 10% in the blend. X-ray studies indicate that the increase of PEI hinders the rapid alignment of naphthalene planes parallel to the surface of the films. The presence of PEI chains in the blend was found to increase the overall friction between the polymer chains in the system and this was found to prevent the formation of highly localized necks. © 1997 John Wiley & Sons, Inc. *J Appl Polym Sci* **65**: 2059–2074, 1997

## INTRODUCTION

Poly(ethylene naphthalate) (PEN) films possess oxygen barrier properties four to five times higher than those of (PET)<sup>1</sup> and they exhibit better thermal, electrical (insulating), and mechanical properties as compared to PET. These characteristics makes PEN attractive for packaging, electrical insulating, and magnetic tape applications, and the demand is expected to increase with the upcoming increase of monomer production.

One of the unusual characteristics of PEN is that it shows necking behavior upon stretching from the amorphous state above the glass transition temperature. In our earlier publication,<sup>2</sup> we reported that this neck formation is a result of a highly localized cooperative orientation of the

naphthalene planes parallel to the surface of the film. This behavior resembles an isotropic to nematic structural transition which occurs at highly localized regions of the sample, thereby manifesting itself as a neck. In this earlier study, we also noted a rapid drop in the measured stretching force accompanying the initial neck formation. This suggested that when the naphthalene planes are aligned parallel to the broad surface of the sample the interchain friction is greatly reduced as a result of this “graphitic” orientation behavior of the naphthalene planes parallel to the broad surfaces of the parts. To counteract this behavior, we undertook the present study wherein we blended PEN with polyetherimide (PEI) in order to increase the friction forces between the PEN chains by introducing stiff and bulky PEI chains into their environment. This molecular-level dispersion of PEI was possible as PEN and PEI exhibit miscibility in the amorphous state at all compositions.<sup>3</sup>

Aside from the scientific curiosity on this unusual neck formation during stretching in the rub-

Correspondence to: M. Cakmak.

\* Current address: SKI Fiber Research Center, Kyungki-do, Korea.

Contract grant sponsor: Eastman Kodak Corp.

*Journal of Applied Polymer Science*, Vol. 65, 2059–2074 (1997)

© 1997 John Wiley & Sons, Inc.

CCC 0021-8995/97/112059-16

bery state, there is a practical importance in studying this behavior. In film processing, this neck formation causes the processing window to be smaller by limiting the production to high draw ratios (uniaxial or biaxial) where films become uniform in thickness once the necks in the films are eliminated. In the following, we summarize our research results on the influence of PEI concentration on the neck formation of PEN/PEI films stretched above the  $T_g$  from amorphous precursors.

## EXPERIMENTAL

### Materials

The poly(ethylene-2,6-naphthalene dicarboxylate) (PEN) with an intrinsic viscosity of 0.86 dL/g used in this study was provided in pellet form by the Eastman Kodak Co. Polyetherimide (PEI) with an intrinsic viscosity of 0.61 dL/g was supplied by the General Electric Co. in pellet form (Ultem 1,000). A series of PEN/PEI blends, ranging from 100/0 to 80/20 in composition, were prepared using a Werner & Pfleiderer corotating twin-screw extruder (ZSK-30). Predried polymer pellets were dry-blended using a tumbler mixer and fed to the hopper of the extruder with an automated feeder. The melt temperature at die was set at 305°C, and the extrudates were subsequently quenched in the water bath and pelletized. The virgin PEN was also passed through the twin-screw extruder to allow it to experience the same thermal history as that of the blends.

### Film Preparation

The pelletized blends were dried and melt-cast using a Prodex 1 in. single-screw extruder equipped with an 8 in. wide sheet casting die and a chill roll take-up device. The temperature of the melt at the die was maintained at 280°C, and the extruded film was quenched on a chill roll. The temperature of the chill roll was maintained at 70°C using a water-circulating temperature control unit. The film take-up speed was about 0.8 m/min, and the thickness of film was controlled between 400 and 500  $\mu\text{m}$ .

### Thermal Analysis

The thermal properties of PEN and its blends with PEI were determined with a Perkin-Elmer

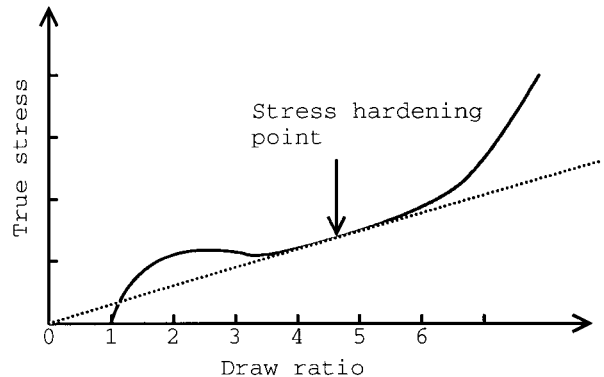


**Figure 1** Determination of the stress-hardening point.

differential scanning calorimeter (DSC-7) at a heating rate of 10°C/min under a dry nitrogen blanket. The temperature scale was calibrated with two standard materials, indium and zinc.

### Density and Crystallinity

A density-gradient column was prepared from the mixtures of the *n*-heptane (density 0.684 g/cc) and the carbon tetrachloride ( $\text{CCl}_4$ , density 1.585 g/cc). The density column was calibrated with a set of standard glass beads after the column reached an equilibrium at 23°C. Density of the sample was measured using the location of the sample, after it reached a stable position in the column.

Crystallinity of the blends was measured by using DSC thermograms. Crystallinity of the blends was normalized to the fraction of PEN present in the blends:

$$\text{Crystallinity (\%)} = \frac{\Delta H_{\text{exp}}}{\Delta H^0} \times 100$$

where  $\Delta H_{\text{exp}} = \Delta H_{\text{melting}} - \Delta H_{\text{cold crystallization}}$  and  $\Delta H^0$  is the heat of fusion for 100% crystalline PEN, 103.4 J/g.<sup>4</sup>

### Stress–Strain Behavior

To determine the uniaxial stress–strain behavior, an Instron tensile tester (Model 4202) with an environmental oven was used. The extruded cast films were cut into 14 mm-wide strips. The tensile tester was operated with the gauge length of 20

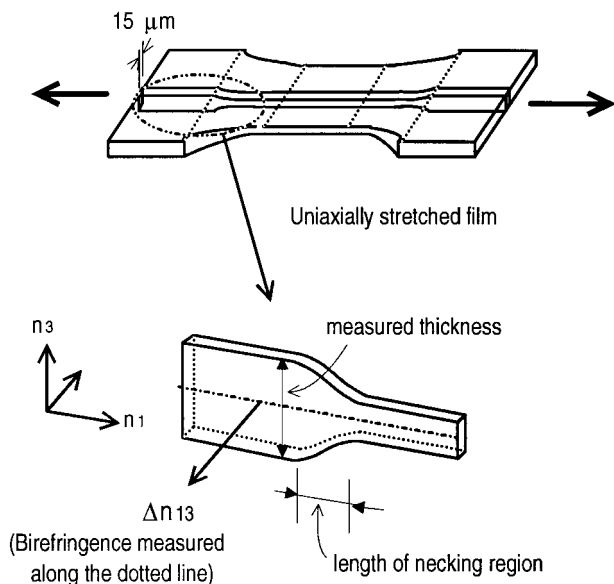


**Figure 2** Procedure of film cutting in the neck region: (1) MD; (2) TD, (3) ND.

mm at two different temperatures,  $T_g + 10^\circ\text{C}$  and  $T_g + 20^\circ\text{C}$ , and with five different strain rates: 50, 100, 200, 500, and 2500%/min.

To construct the true stress–strain curve, true stress was calculated from the measured tensile force using the affine deformation assumption ( $A \times L = A' \times L'$ ). The stress-hardening point is determined from the following procedures: First, the true stress–strain curve is constructed. Sec-

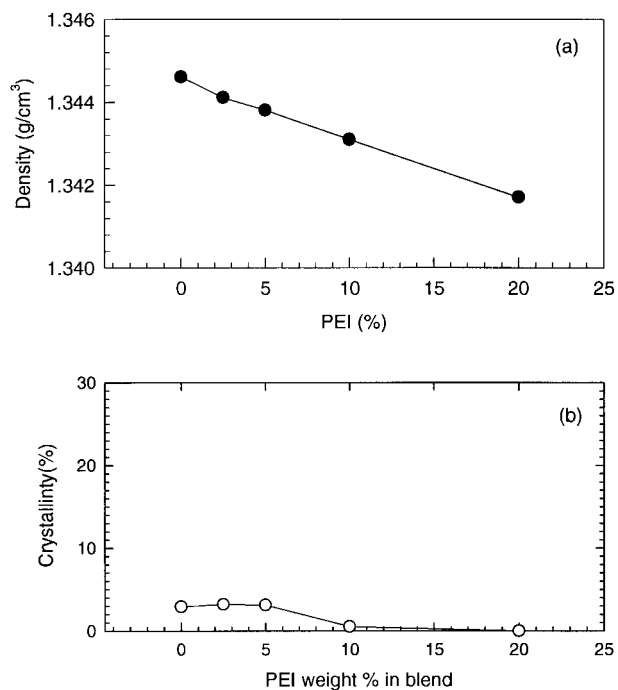


**Figure 4** Density and crystallinity of undrawn films: (a) measured by density gradient column; (b) measured by DSC.

ond, a straight line is drawn passing through the origin and the first tangent point on this curve from the negative side as shown in Figure 1. The strain or draw ratio at this point is taken as the stress-hardening point.

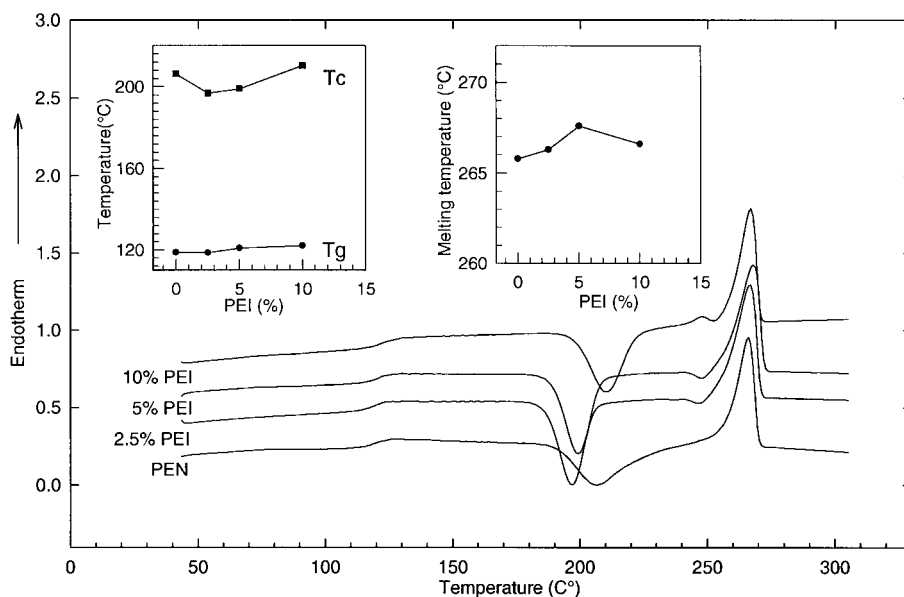


**Figure 3** Thermal properties of PEN/PEI blend films before drawing.

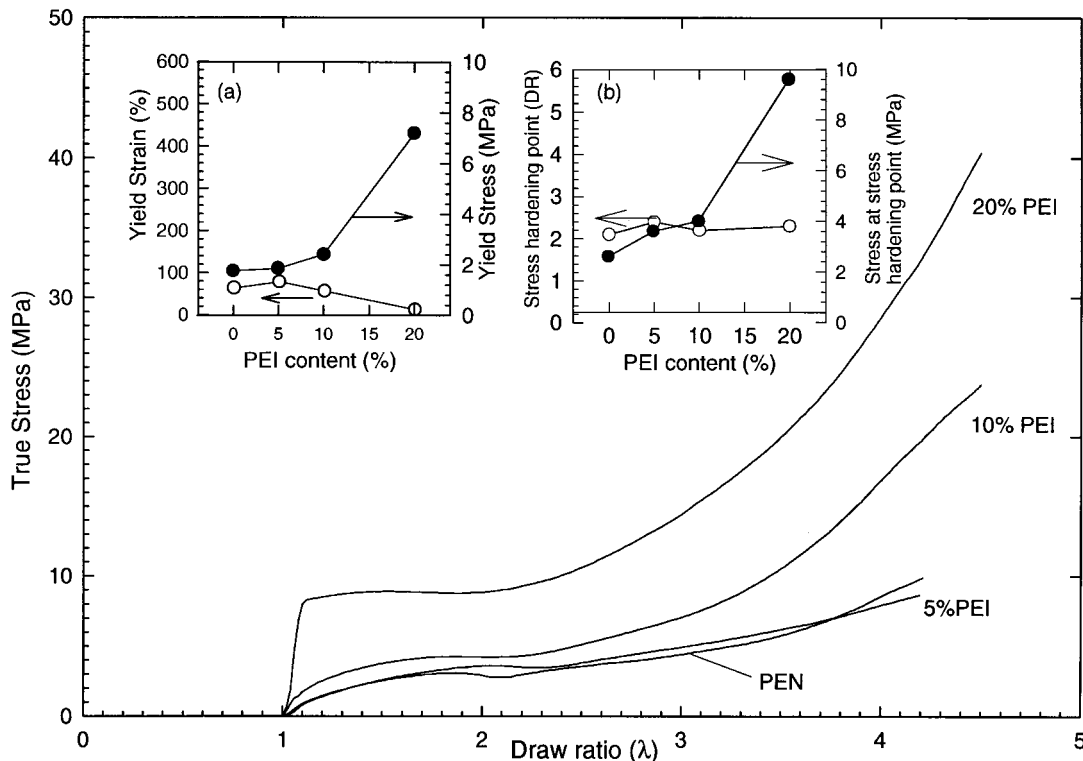


**Figure 5** Stress–strain curves of PEN/PEI blends in uniaxial mode. Draw temperature:  $T_g + 20^\circ\text{C}$ ; draw ratio: 1200%/min.

### Wide-angle X-ray Diffraction

A 12 kW rotating anode generator (Model RU200B) equipped with a Rigaku horizontal diffractometer was used to obtain WAXS profiles of the samples. The X-rays, generated at the copper target, were monochromatized using a graphite monochromator to obtain the  $\text{CuK}\alpha$  wavelength. The goniometer was operated with a step-scanning mode using a  $0.02^\circ/\text{s}$  step interval.

### Microbeam WAXS Studies at the Neck Region

A matrixing microbeam WAXS camera, which was developed in our laboratory, was used to obtain the WAXS patterns along the neck region of the films. This microbeam WAXS camera is specially designed to obtain the scattering patterns from an area as small as  $100\ \mu\text{m}$  diameter. The sample is mounted on a precision X–Y stage to control the sample positions precisely and to maintain spatial registry between the series of WAXS patterns obtained. The camera was mounted on a Rigaku 12 kW rotating anode generator which was operated at 40 kV and 150 mA. A

nickel filter was used to obtain a  $\text{CuK}\alpha$  beam and a  $100\ \mu\text{m}$  diameter collimator was used.

### Birefringence Distribution at the Neck Region

The films containing the neck were generated by stretching the as-cast amorphous films uniaxially to twice of their original gauge length. These samples are rapidly cooled to room temperature. The neck regions were cut in the MD–ND plane using a Reichert histostat rotary microtome to a thickness of  $15\ \mu\text{m}$ . Figure 2 illustrates this procedure.

Birefringence measurements were carried out using a Leitz polarizing microscope (Labolux 12 Pol S) equipped with a  $30\ \lambda$  Berek compensator. Birefringence,  $\Delta n_{13}$  (1 = machine direction, 3 = normal direction), was measured at a series of positions along the machine direction on the center line indicated in Figure 2.

## RESULTS AND DISCUSSION

### Thermal Properties of the As-Cast Films

The sheets cast from the prepared blends all exhibit a single glass transition temperature as

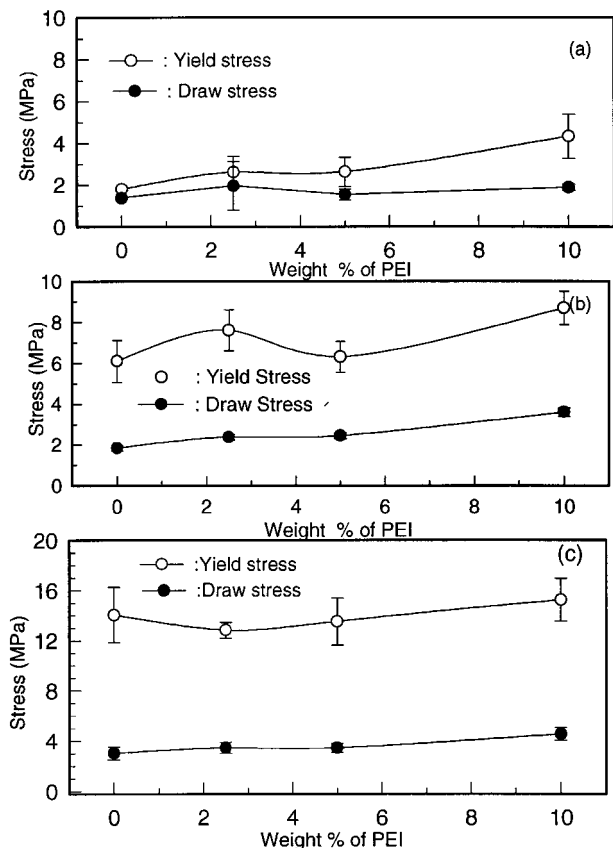


**Figure 6** Yield stress and draw stress of PEN/PEI blend films. Draw temperature:  $T_g + 10^\circ\text{C}$ . (a) Draw rate: 50%/min; (b) draw rate: 500%/min; (c) draw rate: 2500%/min.

shown in their DSC curves in Figure 3. This glass transition temperature increases slightly with the addition of PEI. The melting temperature was observed to increase first and then decrease as the PEI fraction in the blend increased (see inset in Fig. 3). This unusual behavior is attributed to the relatively low melt temperature ( $310^\circ\text{C}$ ) used for the film-casting process as compared to its equilibrium melting point ( $T_m^0 = 337^\circ\text{C}^5$ ). The PEN/PEI blends do not follow the normal melting point depression phenomenon until they are melted over  $340^\circ\text{C}$ . This may be explained as follows: The presence of PEI helps the PEN crystal to survive in the form of a small crystallite or frozen ordered state above the normal melting temperature by increasing the viscosity of the melt. These remaining crystallites or the frozen ordered states in the quenched as-cast films act as nuclei during the subsequent crystallization stage at lower temperatures during the DSC scan. Because of this earlier start of the crystallization during the heat-

ing of a DSC scan, crystals have more of a chance to be larger in size or to be more perfect, which, in turn, increases the melting temperature. However, since the PEI act not only as templates for nucleation but also as a diluent at large concentrations, the melting temperature shows the maximum value at about 5% concentration of PEI. Beyond this point, the dilution effect plays a significant role in reducing the crystallizability of the PEN. In fact, the experiments that we have performed on the thermal crystallizability indicated that blends containing more than 20% PEI significantly lost their ability to crystallize. In addition, the cold-crystallization peak temperature decreases first and subsequently increases as the PEI concentration increases. This also is in accord with the melting temperature behavior mentioned above.

The density of the as-cast films decreases with the increase of lower-density PEI fraction. These melt-cast films are essentially amorphous as determined by DSC (see Fig. 4).

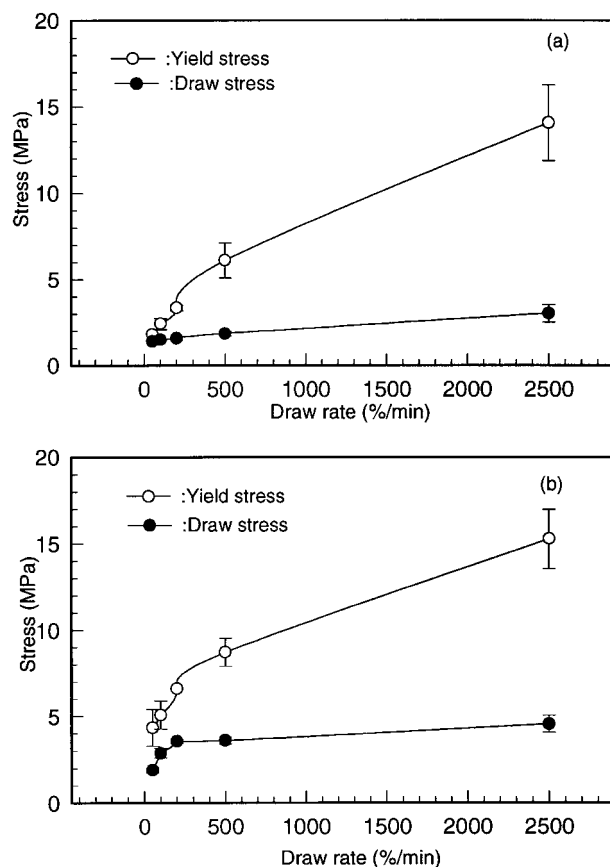


**Figure 7** Yield stress and draw stress of blend films vs. draw rate. Draw temperature:  $T_g + 10^\circ\text{C}$ . (a) Virgin PEN film; (b) 10% PEI film.

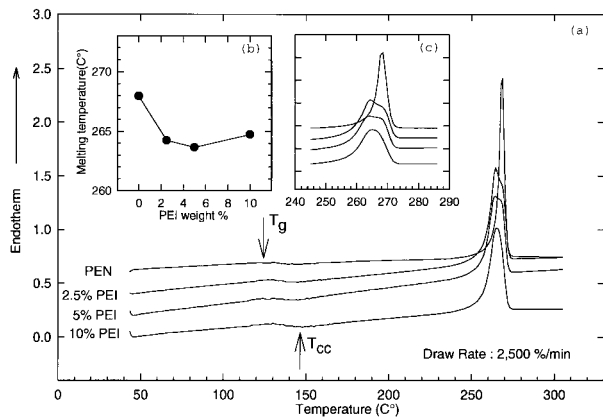


**Figure 8** DSC measurement after drawing at  $T_g + 10^\circ\text{C}$ .

### Effect of PEI and Draw Rate on Stress–Strain Behavior

To ascertain the influence of PEI on the deformation behavior of the PEN/PEI blends, the cast amorphous films were stretched  $20^\circ\text{C}$  above the  $T_g$  of each blend and the stress–strain behavior was recorded and converted to true stress–draw ratio curves (Fig. 5).

After the initial rise, PEN exhibits a rapid drop in the stress at  $\lambda = 2.05$ . This drop in stress coincides with the first appearance of the neck. A further increase in deformation causes a steady increase of stress which results in propagation and eventual disappearance of the neck. This occurs when the slope of this curve begins to increase rapidly. The addition of PEI causes an overall increase in stress, particularly beyond a 95/5 PEN/PEI composition. This rise in stress is also accom-

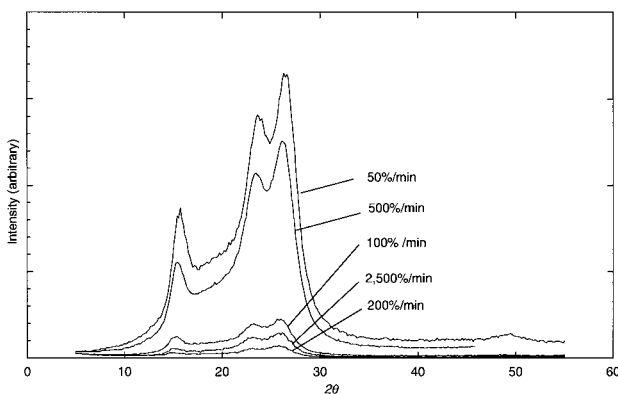


**Figure 9** Wide angle X-ray profiles of PEN film which were drawn at different draw rate. Equatorial reflection mode

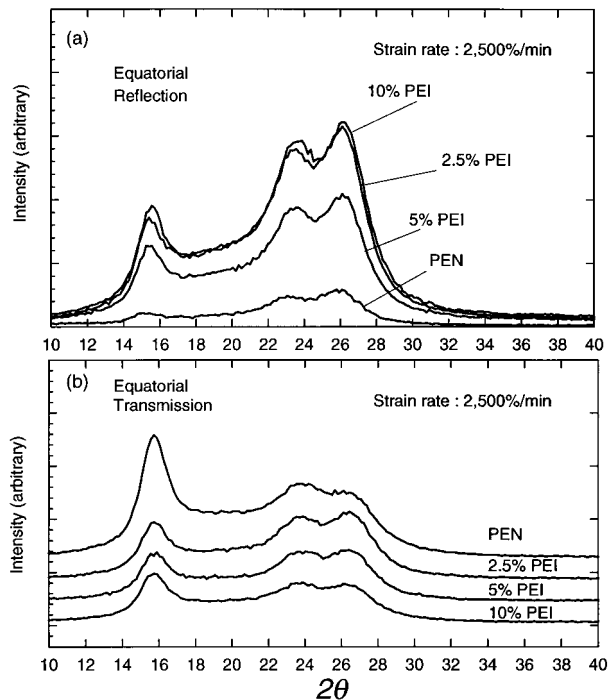


**Figure 10** WAXS profiles of PEN/PEI blend films of different PEI fractions. Films were stretched at 2500%/min draw ratio. (a) Equatorial reflection mode; (b) transmission mode.

panied by the disappearance of the stress drop after the yield. This becomes more evident at 10 and 20% PEI concentrations.

The increase of the PEI fraction causes the increase in the stress. The yield stress increases with the PEI fraction, while the yield strain decreases as shown in Figure 5(b). The stress at the stress-hardening point significantly increased as the PEI in blends increased, but the strain at the onset of stress hardening remained relatively unchanged.

To observe the effect of PEI on the stress–strain behavior systematically, four different PEI concentrations, 0–10% PEI, and five different stretch rates, 100–2500%/min, were selected. Figure 6 shows that the yield stress increases as the PEI fraction increases for all the draw rates that we have investigated. The drawing stress also increases with PEI fraction, but more gradually as compared to the yield stress.

The yield stress and the drawing stress are known to be a function of the draw rate. Allison and Ward<sup>5</sup> reported that the PET showed a linear increase of yield stress as the strain rate increased. However, the drawing stress did not increase monotonically. They concluded that the

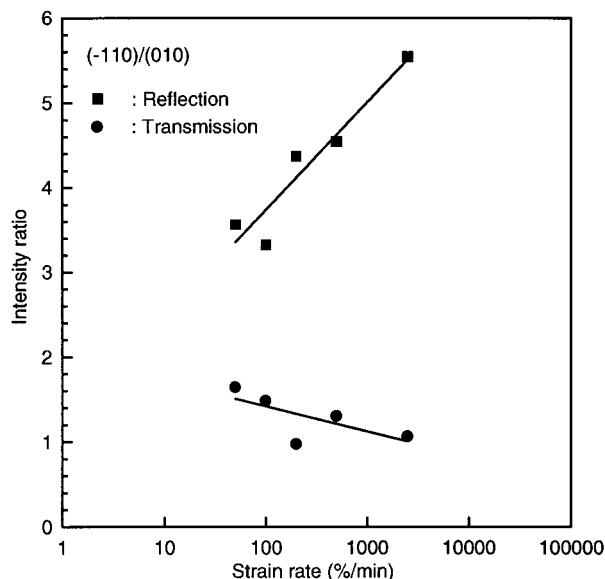


**Figure 11** The ratio of the integrated intensities of  $(-110)$  and  $(010)$  planes in transmission and reflection modes. Equatorial scan.

adiabatic heat generation affects the drawing process but not the yield process. On the other hand, our experimental results indicate that yield stress and the drawing stress increase monotonically as the draw rate increases regardless of the PEI concentration in the blends [see Fig. 7(a) and (b)]. However, the change of drawing stress is quite small compared to that of yield stress.

### Phase Behavior in Drawn Films

#### Thermal properties

Figure 8 shows the DSC thermogram of the films drawn to  $5.0\times$  at  $T_g + 10^\circ\text{C}$  of each blend. The glass transition and cold-crystallization temperatures are still discernible at this high stretch ratio. The area under the cold-crystallization peak increases with increase of the PEI fraction in the blend, indicating that although the films are stretched to the same high stretch ratio an increased proportion of oriented PEN chains remain amorphous with increase of the PEI fraction. These, in turn, crystallize during the DSC scan.

The melting temperature of the films decreases with the increase of PEI fraction as shown in Figure 8(b). Moreover, the melting regions of samples with 2.5 and 5% PEI are composed of two peaks. The presence of double melting peaks suggests the presence of another population of crystals, which melt at a lower temperature than that

of regular PEN crystals. There may be two possible explanations about these low-melting PEN crystals. First, during the stress-induced crystallization, the bulky and noncrystallizable PEI molecules dispersed among the PEN molecules would cause imperfections in the surrounding PEN regions which would cause generation of a lower melting population of PEN crystals as well as normal PEN crystals. A second cause could be the development of a new crystalline phase with a higher melting temperature. However, the X-ray experimental results, which will be discussed below, showed that there is no evidence of another crystal form beside the  $\alpha$ -form crystal. Therefore, the first explanation for the existence of the double melting peaks is more reasonable.

#### Crystal Structures After the Drawing

Figures 9 and 10 are some of the experimental results of the WAXS profiles on the stretched films of PEN and its blends. PEN may possess either the  $\alpha$  and the  $\beta$  crystal forms.<sup>6,7</sup> Our studies indicate that all the films stretched uniaxially from an amorphous precursor exhibit the  $\alpha$  crystal form regardless of the PEI fraction.

PEN films have been reported<sup>2</sup> not to show transverse isotropy when they are subjected to uniaxial unconstrained stretching. This is due to the preferential orientation of the naphthalene

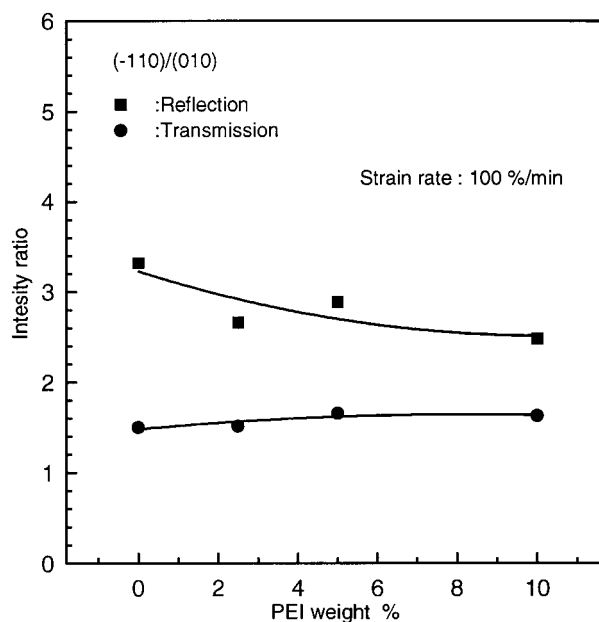


**Figure 12** Intensity ratio of  $(-110)$  plane/ $(010)$  plane. Strain rate: 100%/min. Equatorial scanning mode.

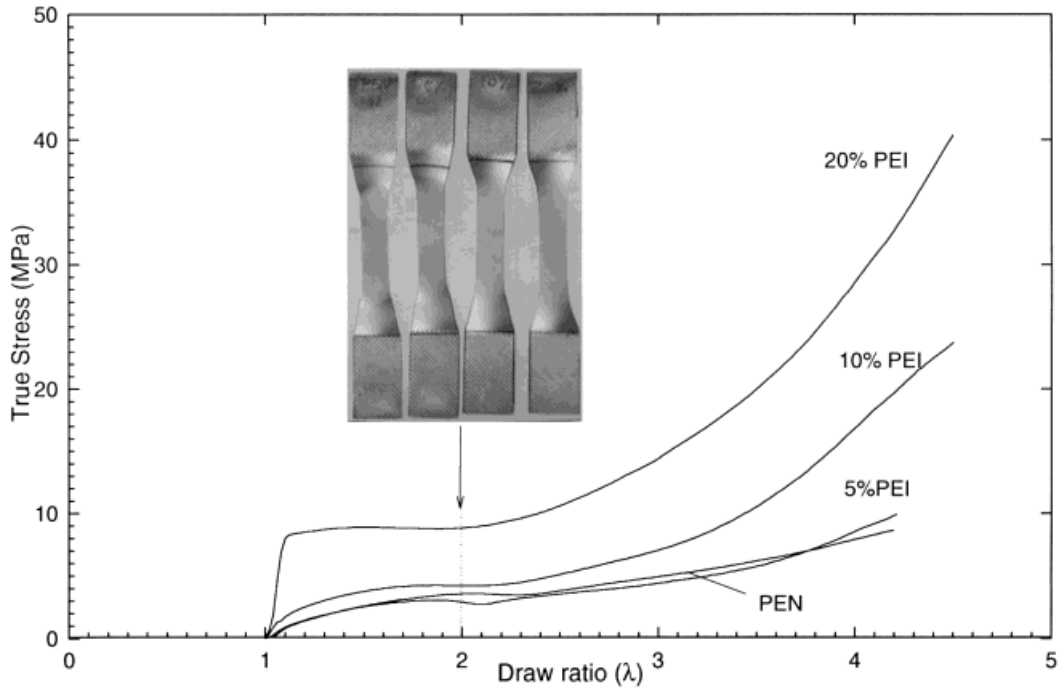


**Figure 13** (a) Stress–strain curves of PEN/PEI films. (b) Film photographs stretched to draw ratio 2. Draw temperature:  $T_g + 20^\circ\text{C}$ , Draw rate: 1200%/min.

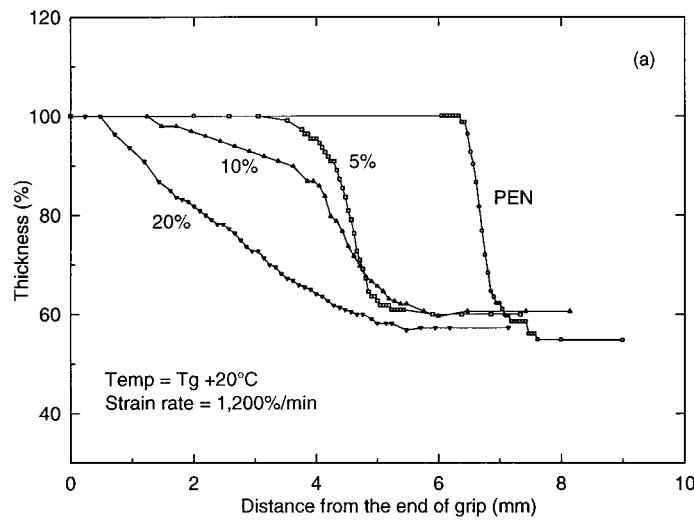
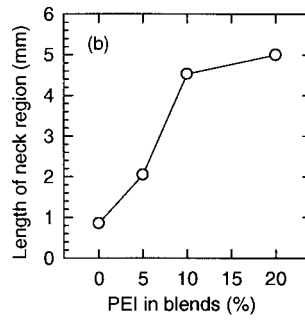


**Figure 14** Thickness change along the neck regions of the blends.



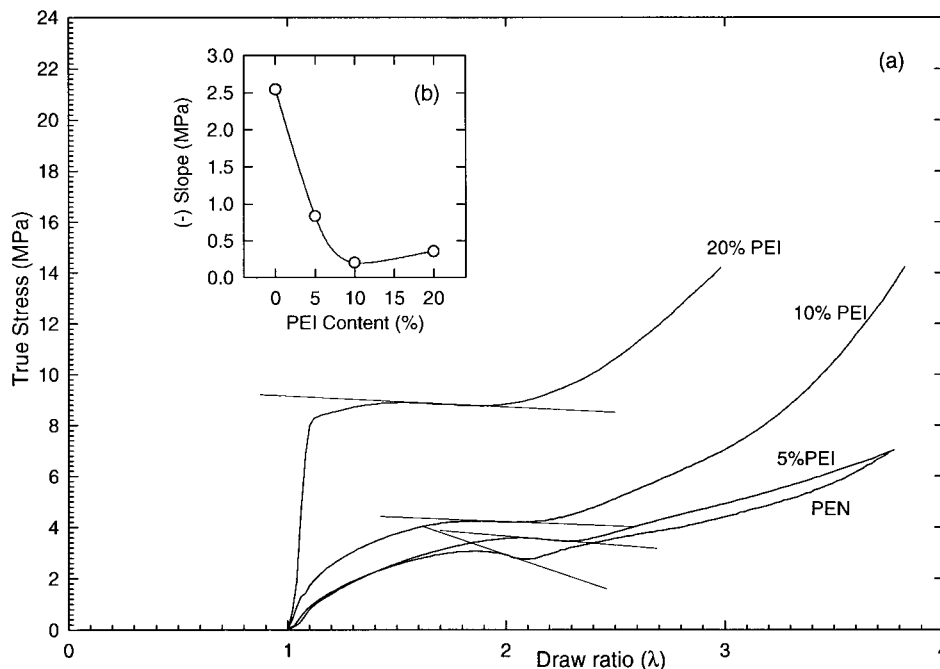


**Figure 15** (a) Uniaxial stress–strain curve showing the magnified view of the start of the deformation. (b) The slope after the yield point vs. PEI content.

planes of PEN parallel to the film surface when the films are stretched. The equatorial wide-angle X-ray profiles on stretched films provide information on such anisotropy. If the stretched films of PEN and its blends exhibit the transverse isotropy, there should not be any difference in the ratios of the peaks between the reflection and transmission mode.

Figure 10(b) shows the WAXS profiles of the stretched films in the transmission mode. PEN and its blend films were stretched to  $5\times$  with a  $2500\%/min$  stretch rate at  $T_g + 10^\circ C$ . These profiles show a clear difference when compared with the profiles of the reflection mode in Figure 10(a). These data also show that the intensity profile differences between transmission and reflection modes become smaller as the PEI fraction increases.

To quantify this orientation behavior, the areas under the peaks of  $(-110)$  and  $(100)$  planes were divided by the area under the peak of the  $(010)$  plane. A peak-separation technique, which uses Pearson VII curves, was applied to the WAXS profiles to obtain the peak areas. Figure 11 shows the  $(-110)/(010)$  ratios obtained in reflection and transmission modes for films processed at different strain rates. This ratio increases in the reflection mode and decreases in the transmission mode as the strain rate increases. This indicated that

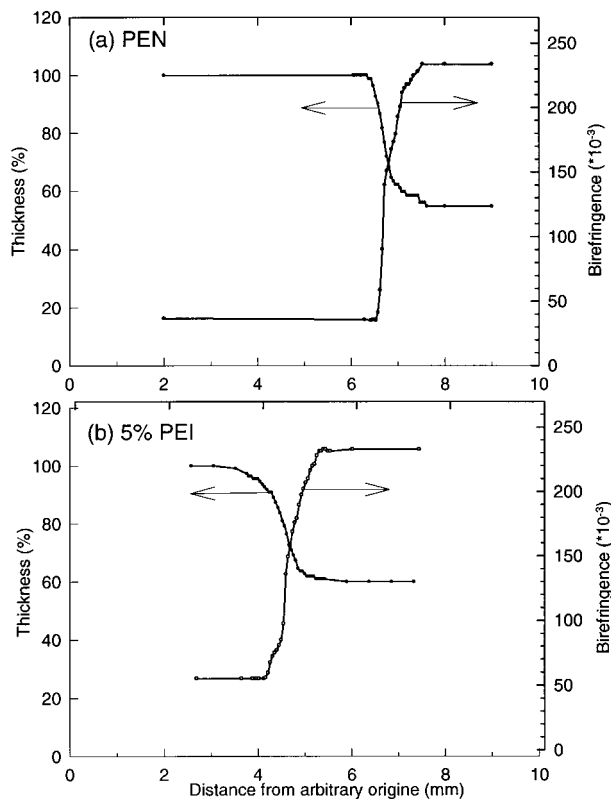


**Figure 16** Normalized thickness and  $\Delta n_{13}$  vs. position along the neck. Films were stretched to  $2\times$  draw ratio. (a) PEN; (b) 5% PEI.

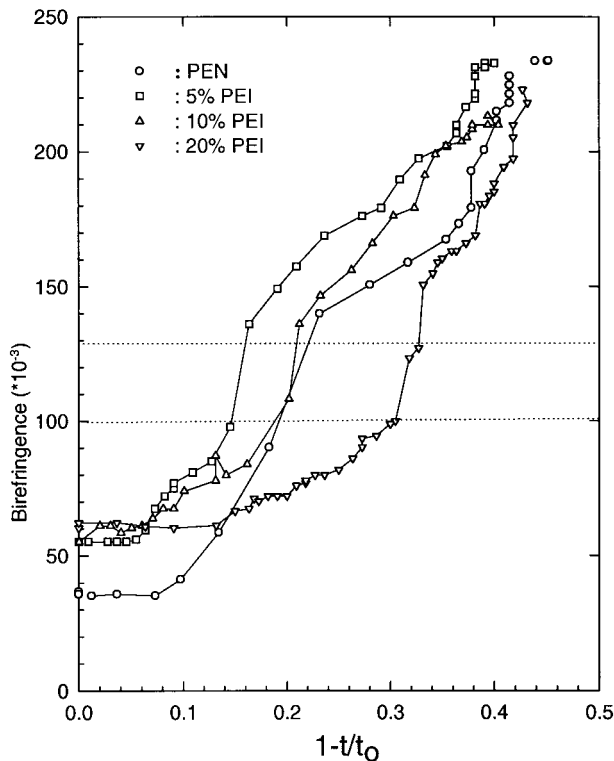
the  $(-110)$  planes become parallel to the film surface as the strain rate is increased. Since the plane of the naphthalene rings corresponds to the  $(-430)$  plane<sup>6</sup> and the  $(-430)$  and  $(-110)$  are nearly parallel to each other (angle between them is  $7.7^\circ$ ), the above results show that the plane of the naphthalene rings becomes increasingly parallel to the film surface as the stretch rate increases.

Figure 12 shows the effect of PEI concentration on the orientation of the naphthalene planes of the PEN crystals. The  $(-110)/(010)$  ratio in the reflection mode decreases and in the transmission mode increases as the PEI in the blends increases. This clearly shows that the tendency for naphthalene planes to orient parallel to the film surface is increasingly disrupted as the PEI concentration increases in the blends. Detailed discussions on the effect of PEI on the orientation behavior of stretched films will be published elsewhere.<sup>8</sup>

### Structure Development in the Neck Region

#### PEI Effect on the Neck Formation

To investigate the PEI effect on the necking phenomenon, a set of the uniaxial drawing conditions



**Figure 17** Birefringence vs. strain in thickness direction.  $t_0$  = initial thickness;  $t$  = thickness at a given position.

was selected. The films were stretched at  $20^\circ\text{C}$  above their respective glass transition temperatures with a  $1200\%/min$  strain rate.

Figure 13 shows the optical photographs of the PEN/PEI blend films, which were stretched at a stretch ratio 2, with their stress–strain curves. At this stretch ratio, a highly localized neck was observed clearly in the PEN sample. However, this local neck turned into a smoother transition region as the PEI fraction in the blends increased. This indicates that the necking of PEN under the uniaxial stretching condition can be eliminated by the addition of PEI.

To fully quantify the influence of the PEI on the neck formation of the PEN and its blend films, the thickness of the films was measured along the neck region. The films were sliced using a microtome in the MD–ND plane as shown in Figure 2. The thickness variation along the machine direction, which is normalized by the initial thickness, is shown in Figure 14. Here, the data indicate that the sharp transition region characteristic of the necking gives way to a smoother transition with increase of the PEI fraction. As a result of this effect, the transition length increases with the increasing fraction of PEI in the blend as shown in Figure 14(b).

Since the necking phenomenon is known to be associated with the yield,<sup>9</sup> the yield points of the true stress–strain curves were analyzed to determine a general relationship between the necking phenomena and the yield point of the films in this study. A region around the yield point in the stress–strain curves are shown in Figure 15(a). The curves show that the stress decreases immediately after the yield point. This is mainly a result of the rapid thinning of the film thickness that accompanies neck formation in the samples. As can be seen in Figure 15(b), the slope of this region related to the mentioned transition length of the neck [see Fig. 14(b)]. Consequently, this slope is a good gauge for a quick evaluation of the presence of the neck in the samples. At about 10% of PEI fraction, this slope becomes essentially zero following the disappearance of the neck in the samples.

#### Birefringence Distribution in the Neck Region

We measured the birefringence profiles of the neck regions along the line at the midplane, as mentioned in Figure 2. This provided the variation of the out-of-plane birefringence  $\Delta n_{13}$  ( $1 = \text{MD}$ ,  $3 = \text{ND}$ ) along the neck regions. This bire-

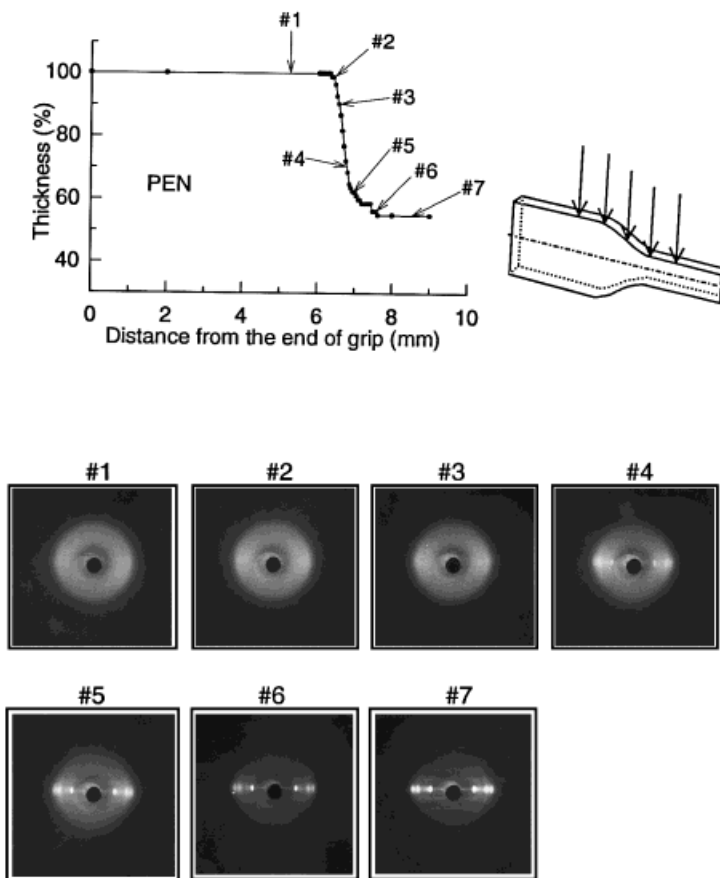


**Figure 18** WAXS patterns taken from normal direction, PEN. Film was stretched to  $2\times$  draw ratio at  $T_g + 20^\circ\text{C}$ . (X-ray beam parallel to normal direction).

fringe data, as well as the thickness change in the neck region, are shown in Figure 16 for four different PEN/PEI compositions.

As the PEI concentration increases, the out-of-plane birefringence changes along the neck region become more gradual following the gradual disappearance of the neck region. To isolate the compositional effects from the deformation effects, we plotted  $\Delta n_{13}$  as a function of deformation in the thickness:  $(1 - t/t_0) = (\Delta t/t_0)$ . The initial slope of the birefringence–deformation curves decrease with increase of the PEI fraction. In addition, in all the materials, we observed a sudden increase of birefringence beyond a critical value of 0.1, as indicated by two horizontal lines in Figure 17. This sudden increase of birefringence points to a critical value of orientation beyond which the naphthalene planes go through a rapid cooperative reorientation like a deck of cards. When the angle between the naphthalene rings and the film surface reaches a certain value, the naphthalene rings rapidly become aligned parallel to the film

surface, and this causes the sudden increase of birefringence. This orientation model was proposed by Cakmak and Lee,<sup>2</sup> and they showed that this explanation is reasonable, especially in the film drawn at lower drawing temperatures. This critical region actually becomes narrower and shifts to larger deformation levels as the PEI concentration increases.

#### *Crystal Structure Variation Along the Neck Region*

To investigate the orientation and phase behavior during the neck formation, a series of WAXS patterns were obtained using a microbeam X-ray device with a  $100\ \mu\text{m}$ -diameter X-ray beam. For this, we chose to investigate 100/0 and 80/20 PEN/PEI blends. These films were stretched at  $T_g + 20^\circ\text{C}$  with a  $1200\%/ \text{min}$  strain rate.

Figures 18 and 19 show the WAXS patterns in the neck region of the PEN film with an X-ray beam along ND and TD directions, respectively. Numbers on the thickness profile in Figure 18(a)

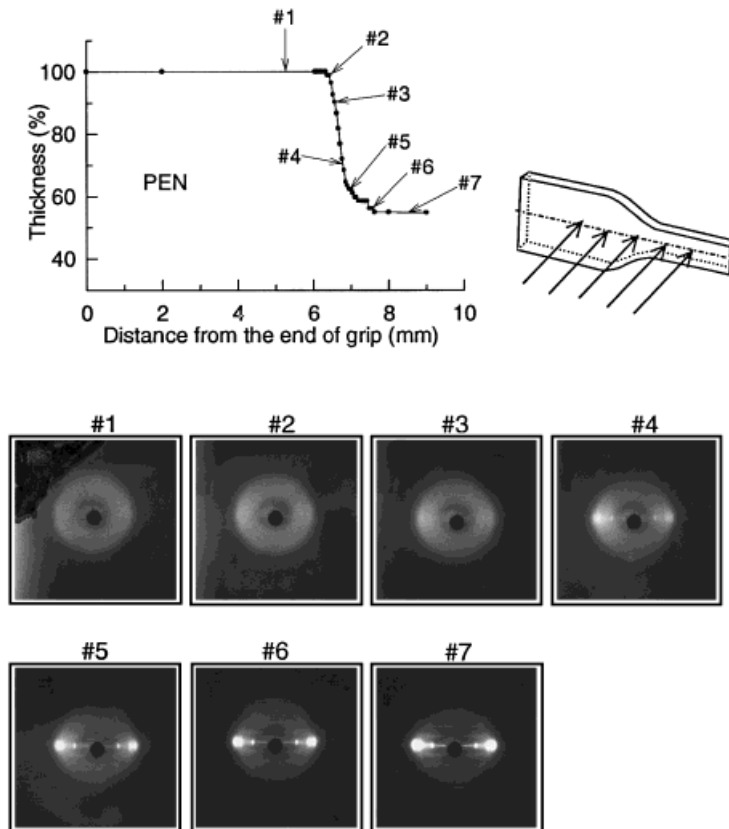


**Figure 19** WAXS patterns taken from transverse direction, PEN. Film was stretched to  $2\times$  draw ratio at  $T_g + 20^\circ\text{C}$ . (X-ray beam parallel to transverse direction).

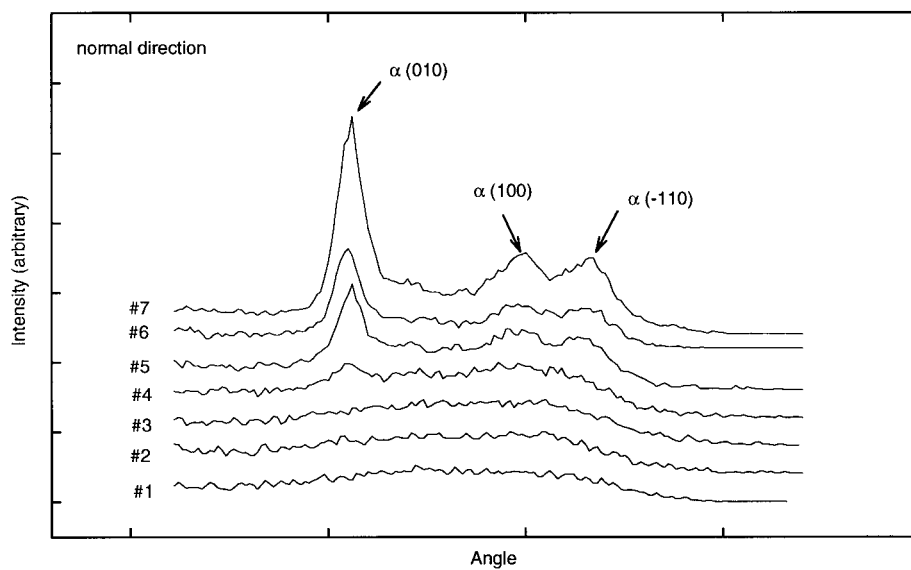


**Figure 20** Intensity profiles from WAXS flat films of the neck region in PEN film. X-ray beam is in normal direction.

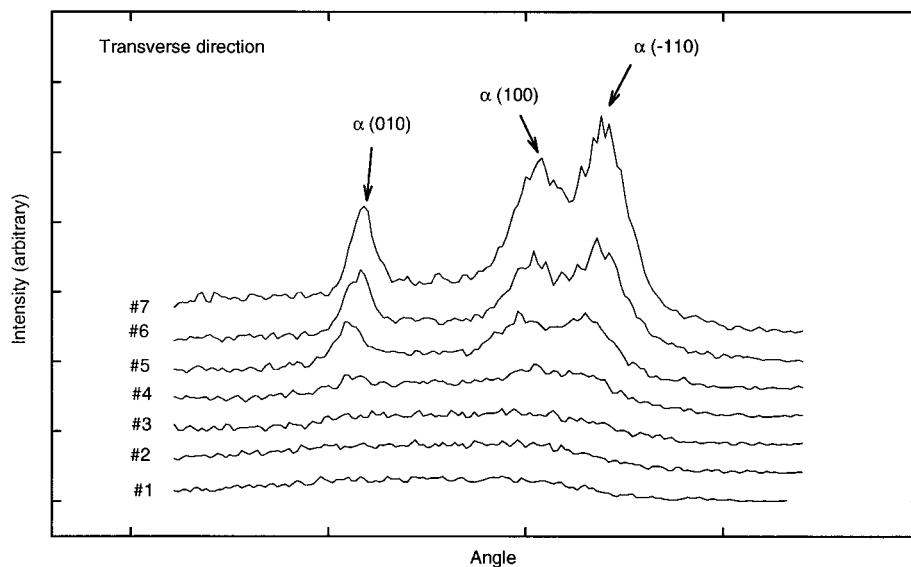


**Figure 21** Intensity profiles from WAXS flat films of the neck region in PEN film. X-ray beam is in transverse direction.

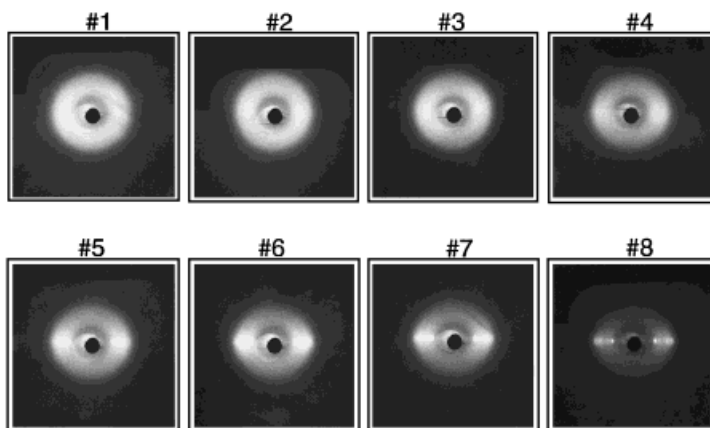
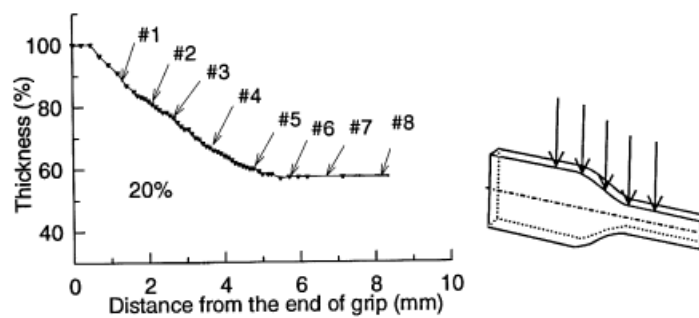


**Figure 22** WAXS patterns taken from normal direction, 20% PEI. Film was stretched to  $2\times$  draw ratio at  $T_g + 20^\circ\text{C}$ .

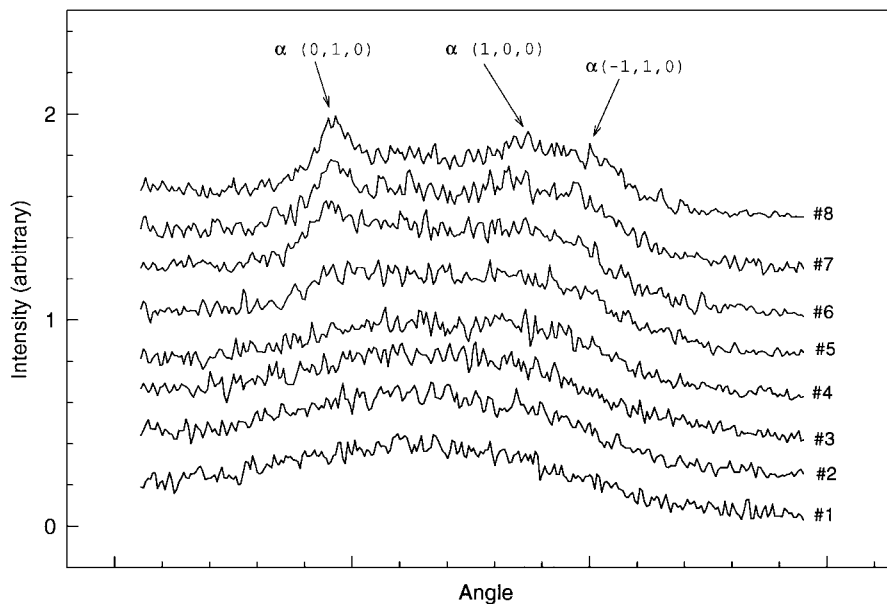


**Figure 23** Intensity profiles from WAXS flat films of neck region 20% PEI. X-ray beam is in normal direction.

indicate the locations where the WAXS patterns were obtained. In the early stages of neck formation (#1–#3), the micro-WAXS film patterns indicate an essentially amorphous structure with increasing concentration of intensity in the equatorial regions. At position #4, some distinct crystalline peaks begin to emerge on the equatorial line. The strongest of these peaks is the  $(-110)$  peak, corresponding roughly to the interplanar correlation of stacked naphthalene planes. At this position, no distinct off-equatorial line diffraction peaks were observed. This indicates that the three-dimensional order is absent at this position and the structure attains a nematic order as a result of preferential orientation of the naphthalene planes parallel to the film surface. The equatorial diffraction spots become stronger in intensity and the spots of off-equatorial planes begin to emerge near the final stages of this transformation. (See the patterns of #4 position and beyond.) An increasing order between #4 and #5 as observed in the X-ray patterns also coincides with region where a rapid birefringence change was observed.

To obtain more detailed quantitative information, intensity profiles of the equator on the WAXS films were obtained using an image processor. In Figures 20 and 21, the X-ray intensity profiles were given for different locations in the neck region. The shapes of the intensity profiles were not much different between the normal direction and

the transverse direction up to position #4. However, the difference between the intensity profiles of the normal direction and the transverse direction became larger toward the final stage of the deformation. The intensity of the  $(010)$  plane becomes dominant when the X-rays are directed in the normal direction, whereas the  $(-110)$  peak becomes dominant when the X-rays are directed in the transverse direction.

Figures 22 and 23 and 24 and 25 are the WAXS patterns and X-ray intensity profiles at the necking region of a PEN/PEI blend film which has 20% PEI. The crystals developed slowly compared with that in virgin PEN film. However, the change of crystalline structure was similar to that of virgin PEN. The diffraction patterns of the crystal were barely observed first at position #6, and this location is also near the position of the sudden increase of birefringence.

## CONCLUSIONS

The melting temperatures of the as-cast PEN/PEI blend films do not follow the normal melting point depression. The melting temperature increases at first with PEI content and shows the highest value at 5% of PEI in the blends. This is due to the melt temperature during the film processing,  $310^{\circ}\text{C}$ , being too low to destroy all the preexisting crystals.

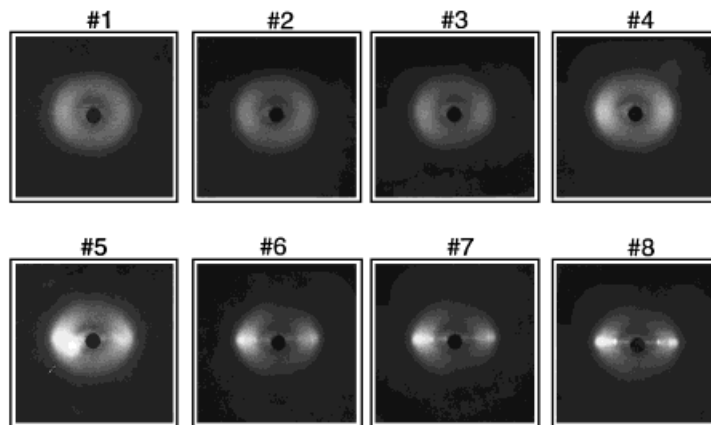
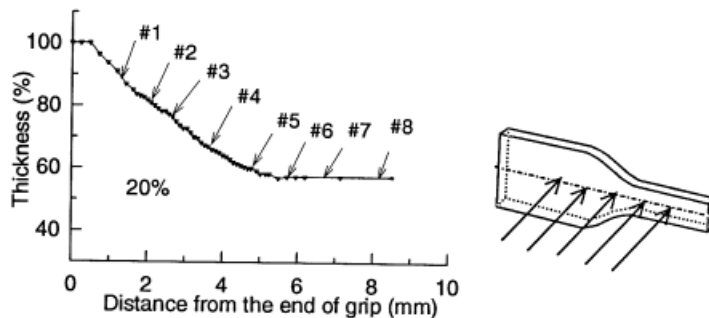


**Figure 24** WAXS patterns taken from transverse direction, 20% PEI. Film was stretched to  $2\times$  draw ratio at  $T_g + 20^\circ\text{C}$ .

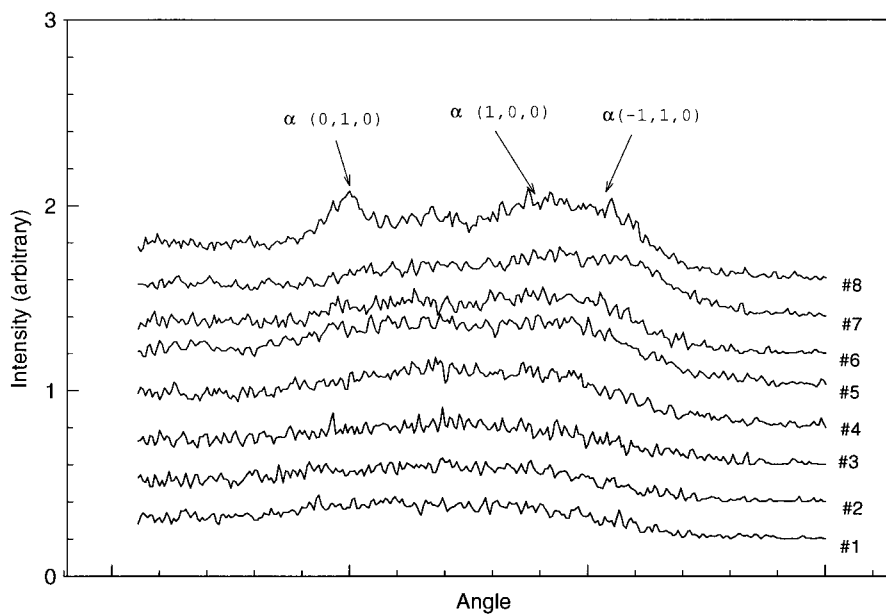


**Figure 25** Intensity profiles from WAXS flat films of neck region, 20% PEI. X-ray beam is in transverse direction.

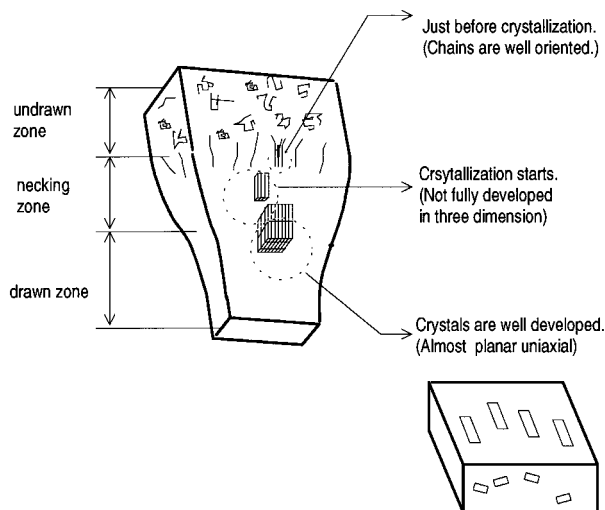


**Figure 26** Model of Structure Development in the neck region.

When the films were drawn, the melting temperature of the blends decreased as the PEI fraction increased. It also showed double melting peaks in the blends of 2.5 and 5% PEI. This double melting is attributed to another population of crystals which are smaller or less perfect than are the normal crystals caused by the presence of PEI.

The yield stress and the draw stress increased as the draw rate or the PEI portion in the blend increased. This indicates that the bulky and stiff PEI molecules hinder the motion of the PEN molecules by creating internal resistance.

PEN shows a sharp necking phenomenon even at 20°C above its glass transition temperature. The addition of PEI was observed to reduce this necking behavior, and the necking behavior disappeared with a PEI fraction of greater than 10% in the blend. The slope between the yield point and the draw point in the true stress-strain curve was found to be a good gauge for an evaluation of the presence of the necking.

The out-of-plane birefringence,  $\Delta n_{13}$ , in the drawn films changes more gradually in the presence of PEI. A critical birefringence was observed beyond which a sudden increase in birefringence occurs. This is attributed to the rapid alignment of naphthalene rings parallel to the film surface over a very short distance.

Wide-angle X-ray diffraction patterns along the neck region shows that the crystallization occurs in the middle of the neck formation. The X-ray intensity profiles in the neck region suggested

that a uniplanar axial texture forms as a result of preferential chain orientation and naphthalene plane orientation. Figure 26 shows the model of the crystal formation during the necking of PEN.

The naphthalene rings are aligned almost parallel to the film surface after the drawing. The higher draw rate gives the naphthalene rings a better alignment parallel to the film surface. However, PEI hinders this alignment of the naphthalene rings and makes the drawn films less anisotropic between normal and transverse directions.

We would like to thank Eastman Kodak Corp. for funding all parts of this project. We also would like to thank Dr. Jehuda Greener for valuable discussions during the course of this research.

## REFERENCES

1. M. E. Stewart, A. J. Cox, and D. M. Naylor, *ANTEC* 93, 1222 (1993).
2. M. Cakmak, and S. W. Lee, *Polymer*, **36**, 4039 (1995).
3. Anon. Res. Discl. 283,677 (1987).
4. S. Z. D. Cheng and B. Wunderlich, *Macromolecules*, **21**, 789 (1988).
5. S. W. Allison and I. M. Ward, *Br. J. Appl. Phys.*, **18**, 1151 (1967).
6. Z. Mencik, *Chem. Prumysl.*, **17**, 78 (1967).
7. S. Buchner, D. Wiswe, and H. G. Zachmann, *Polymer*, **30**, 480 (1989).
8. M. Cakmak, J. C. Kim, to appear.
9. I. M. Ward, *Mechanical Properties of Solid Polymers*, Wiley, Chichester, 1983, Chap. 11.